

Article

# Sr<sup>2+</sup> Ion Substitution Enhanced Dielectric Properties of Co<sub>(2)</sub>Z Ferrites for VHF Antenna Substrate

Ji Wang<sup>1</sup>, Kunlong Li<sup>2,\*</sup> and Gongwen Gan<sup>3</sup>

<sup>1</sup> School of Management and Economics, University of Electronic Science and Technology of China, Chengdu 610054, China

<sup>2</sup> School of Mathematical Science, University of Electronic Science and Technology of China, Chengdu 610054, China

<sup>3</sup> School of Information Science and Technology, Southwest Jiaotong University, Chengdu 611756, China

\* Correspondence: likunlong2013@163.com

**Abstract:** The effect of Sr<sup>2+</sup> ions on the microstructure and high frequency properties of 2.5 wt% Bi<sub>2</sub>O<sub>3</sub> added to Co<sub>(2)</sub>Z hexaferrites (3Ba<sub>(1-x)</sub>Sr<sub>x</sub>O•2CoO•12Fe<sub>2</sub>O<sub>3</sub>, x = 0.0, 0.2, 0.4 and 0.6) synthesised using the solid-state reaction method was investigated. Experimental results indicate that the dielectric properties were markedly enhanced with the increase in the content of Sr<sup>2+</sup> ions, thereby increasing the miniaturisation factor, which enables a size reduction in a long frequency range. Slight changes to saturation magnetisation ( $M_s$ ) and coercivity ( $H_c$ ) were observed, i.e., the saturation magnetisation ( $M_s$ ) decreased from 39.99 to 38.11 emu/g, and coercivity ( $H_c$ ) increased from 59.05 to 65.21 Oe when  $x$  increased from 0.0 to 0.6. Meanwhile,  $\epsilon'$  increased from approximately 8 to 12, indicating the invariability in  $\mu'$ . In addition, the processed materials exhibit relatively low magnetic loss and dielectric loss (magnetic loss  $\tan\delta_\mu \approx 0.08$  and dielectric loss ( $\tan\delta_\epsilon \approx 0.007$ )). These results indicate that the substituted CO<sub>(2)</sub>Z ferrites have excellent potential in high-frequency antenna applications.

**Keywords:** Co<sub>(2)</sub>Z hexaferrites; miniaturisation factor; permeability; dielectric properties; low loss



**Citation:** Wang, J.; Li, K.; Gan, G. Sr<sup>2+</sup> Ion Substitution Enhanced Dielectric Properties of Co<sub>(2)</sub>Z Ferrites for VHF Antenna Substrate. *Metals* **2022**, *12*, 1541. <https://doi.org/10.3390/met12091541>

Academic Editors: Haiming Ding, Peng Wang and Xiangguang Kong

Received: 6 July 2022

Accepted: 14 September 2022

Published: 18 September 2022

**Publisher's Note:** MDPI stays neutral with regard to jurisdictional claims in published maps and institutional affiliations.



**Copyright:** © 2022 by the authors. Licensee MDPI, Basel, Switzerland. This article is an open access article distributed under the terms and conditions of the Creative Commons Attribution (CC BY) license (<https://creativecommons.org/licenses/by/4.0/>).

## 1. Introduction

The rapid development of information and communication technology has led to greater demand on the size and properties of modern communication equipment. Lightweight, high-performance ferrite-based antennas play important roles in wireless communication systems. Another important factor is the miniaturisation of antennas, which has become the topic of recent research [1–3]. However, one problem is miniaturisation of the antenna negatively affects the performance of the wireless communication system. Thus, the search for a range of new approaches to determine size and performance is urgent. One method to achieve miniaturisation is to increase the miniaturisation factor, which depends on the refractive index ( $n = (\mu'\epsilon')^{1/2}$ , where  $\mu'$  and  $\epsilon'$  are actual parts of permeability and permittivity, respectively). Therefore,  $n$  increases as the value of  $\mu'$ ,  $\epsilon'$  or both increases [4]. However, this approach is insufficient in the reception and transmission process of electromagnetic waves, as matching impedance between the antenna substrate and free space weakens the excitation of the surface wave, which is the key to mutual coupling between antenna arrays, causing deterioration of antenna radiation performance [5–7]. Therefore, adjusting the impedance of the antenna substrate to achieve impedance matching is important to ensuring the radiation performance of the antenna. The impedance ( $Z$ ) of electronic materials is closely correlated to  $\mu'$  and  $\epsilon'$ , according to the definition of  $Z$  in the following equation [8]:

$$Z = \eta_0(\mu' / \epsilon')^{1/2} \quad (1)$$

where  $\eta_0$  is the impedance of free space. If  $\mu'$  and  $\epsilon'$  values could be tailored to become close or equal to each other, then  $Z$  becomes close to  $\eta_0$ . In addition, low loss properties

are equally important for the antenna substrate material, as loss control is of paramount importance to reducing energy consumption [9–11]. Therefore, ferrite materials are ideal for antenna substrate applications that possess  $\mu'$  and  $\epsilon'$ , relatively high working frequency and low magnetic and dielectric loss.

The soft magnetic material  $\text{Ba}_3\text{Co}_2\text{Fe}_2\text{O}_{41}$  (Co2Z) hexaferrite has been broadly used in high-frequency devices owing to its high intrinsic magnetic anisotropy field, moderate saturation magnetisation and permittivity [12–14]. It has high permeability and low loss properties in the range of terrestrial digital multimedia broadcasting (T-DMB) frequency [15], and its crystal structure consists mainly of stacked layers of tetrahedral and octahedral  $\text{Fe}^{3+}$  sites shared by  $\text{Co}^{2+}$  ( $3d^7$ ) ions. The high-temperature magnetoelectric coupling is ascribed to magnetic  $\text{Co}^{2+}$  ( $3d^7$ ) ions contributing to enhancing the electronic exchange strength [16]. Nanomaterials play important roles in various applications including energy, biomedical, sensing and pharmaceuticals [17–19]; recent research has focused on  $\text{Co}_{(2)}\text{Z}$  barium ferrites to tailor the magnetic–dielectric properties through substituting  $\text{Ba}^{3+}$  ions using other ions by introducing nanomaterials. Amongst them,  $\text{Sr}^{2+}$  ion substitution is considered an effective method to adjust the magnetic–dielectric properties [20,21]. In addition,  $\text{Bi}_2\text{O}_3$  sintering aids can not only lower sintering temperature but also tailor magnetic–dielectric properties of  $\text{Co}_{(2)}\text{Z}$  barium ferrites. Harris et al. investigated how  $\text{Bi}_2\text{O}_3$  aids modified M-type barium ferrites to achieve equal permeability and permittivity over a long frequency range. Our previous research explored the effect of ion substitution on the adjustment of magnetic properties of M-type barium ferrite, as well as  $\text{Bi}_2\text{O}_3$  aids on the sintering temperature and ferrite densification [22,23]. Results showed that combined with the excellent tuneable characteristics of  $\text{Co}_{(2)}\text{Z}$  barium ferrites, improving high-frequency electromagnetic characteristics by ion substitution is an effective method to achieve matching permeability and permittivity as well as high miniaturisation factor. Here,  $3\text{Ba}_{(1-x)}\text{Sr}_x\text{O}\bullet 2\text{CoO}\bullet 12\text{Fe}_2\text{O}_3$  ( $x = 0.0, 0.2, 0.4$  and  $0.6$ ) ferrites with 2.5wt%  $\text{Bi}_2\text{O}_3$  were prepared. The magnetic–dielectric properties of the resultant materials were studied to achieve equal permeability and permittivity and low loss properties over a long frequency band in the high frequency range [24].

## 2. Experiment and Measurement

### 2.1. Materials and Methods

$\text{Sr}^{2+}$  ion-substituted  $\text{Co}_{(2)}\text{Z}$  barium ferrites  $3\text{Ba}_{(1-x)}\text{Sr}_x\text{O}\bullet 2\text{CoO}\bullet 12\text{Fe}_2\text{O}_3$  with added 2.5 wt%  $\text{Bi}_2\text{O}_3$  were synthesised using analytical grade  $\text{BaCO}_3$  (AR grade,  $\geq 99\%$ ),  $\text{Fe}_2\text{O}_3$  (AR grade,  $\geq 99.5\%$ ),  $\text{Co}_2\text{O}_3$  (AR grade,  $\geq 99.5\%$ ),  $\text{SrO}$  (AR grade,  $\geq 99\%$ ) and  $\text{Bi}_2\text{O}_3$  (AR grade,  $\geq 99.5\%$ ). Subsequently, the objective products were synthesised through the conventional solid-state reaction method. The raw powders were mixed in a ball mill for 10 h, with zirconia balls and deionised water as the milling media. Then, the mixed powders were dried and pre-sintered at  $1150\text{ }^\circ\text{C}$  for 4 h in a muffle furnace.  $\text{Bi}_2\text{O}_3$  was added to the pre-sintered powder and then milled once more for 12 h. After drying, the milled powders were pelleted by adding 10 wt% polyvinyl alcohol (PVA) and then pressed into thick plates and rings. Finally, the dense samples were sintered at  $925\text{ }^\circ\text{C}$  for 4 h.

### 2.2. Measurements

The phase constitution of the ferrites was detected by an X-ray diffractometer (XRD, DX-2700, Haoyuan Co., Chengdu, China) with  $\text{Cu-K}\alpha$  radiation. The microtopography of the ferrite surface was detected using a scanning electron microscope (SEM, JEOL, JSM-6490, Tokyo, Japan). The complex permeability and dielectric constant were measured with a HP-4291BRF impedance analyser (Agilent, Santa Clara, CA, USA). The bulk density was measured using an auto density tester (GF-300D, AND Co., Tokyo, Japan) based on Archimedes' principle. A vibrating sample magnetometer (VSM, EZ Model 10, MicroSense, Encinitas, CA, USA) was used to measure the magnetisation hysteresis loops. All measurements were performed at room temperature.

### 3. Results and Discussion

#### 3.1. SEM

Surface topography of cross sections of the ferrite samples with different  $\text{Sr}^{2+}$  ion substitution  $x$  values is displayed in Figure 1. On the one hand, a marked change in the average grain size is observed, indicating that as the content of substituted  $\text{Sr}^{2+}$  ions increases, the average grain size shows a downward trend. The average grain size can be calculated as 1.03, 0.89, 0.67 and 0.61  $\mu\text{m}$  for different  $x$  values using a statistical method with the following formula [25]:

$$G_a = \frac{1.5 L}{M N} \quad (2)$$

where  $L$  is the total line length, and  $M$  and  $N$  are the magnification and the total number of intercepts, respectively. The decrease in grain size with the increase in  $\text{Sr}^{2+}$  ion substitution is due to the smaller ion radius of  $\text{Sr}^{2+}$  ions than that of  $\text{Ba}^{2+}$ ; small ion radius always causes low grain size [26]. On the other hand, with the increase in  $\text{Sr}^{2+}$  ion substitution, more pores are observed due to the increased difficulty in crystallisation and clusters of grains [27].

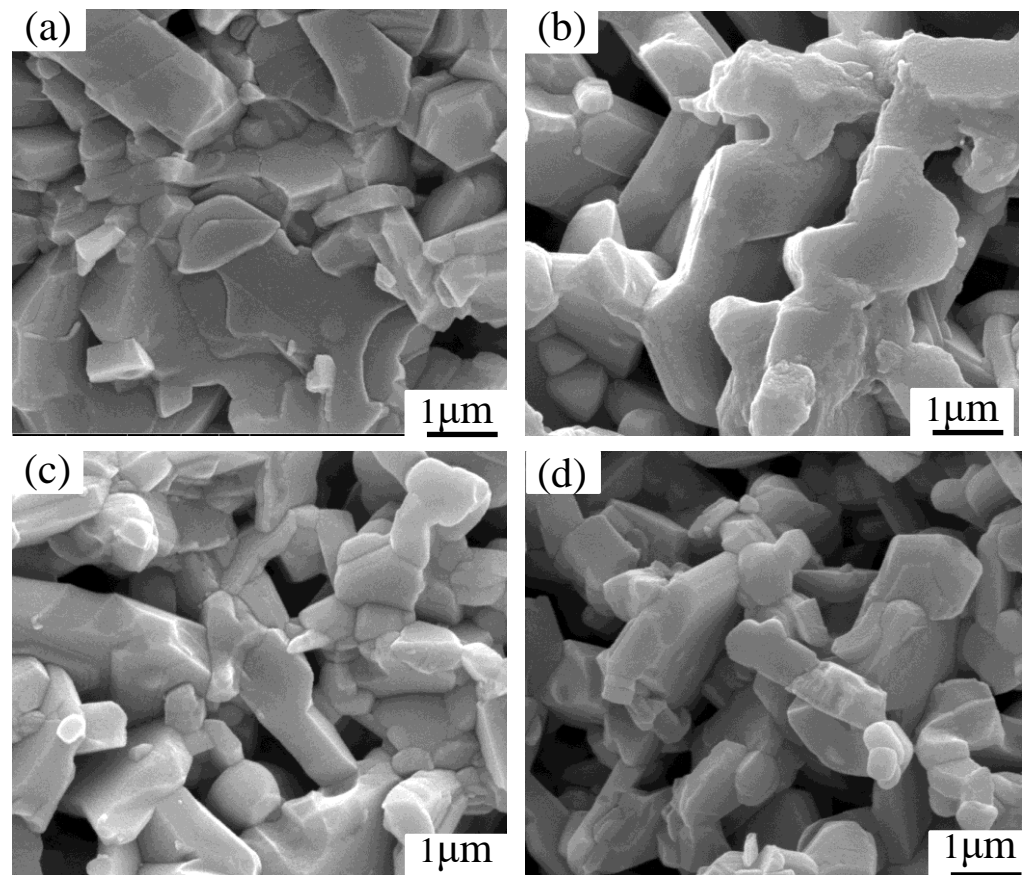


**Figure 1.** SEM images of the materials with different  $\text{Sr}^{2+}$  ion substitution  $x$  values. (a)  $x = 0.0$ , (b)  $x = 0.2$ , (c)  $x = 0.4$  and (d)  $x = 0.6$ .

#### 3.2. XRD

The XRD patterns of the ferrites with different  $\text{Sr}^{2+}$  ion substitution  $x$  values are shown in Figure 2. Normal  $\text{Co}_{(2)}\text{Z}$  barium ferrite phase can be obtained by adding 5 wt%  $\text{Bi}_2\text{O}_3$  aids, from which the peaks with normal  $\text{BaFe}_{12}\text{O}_{19}$  phase and  $\text{BiFeO}_3$  phase can be obtained, indicating no other phase or structure generated during the sintering process.

The formation of the  $\text{BiFeO}_3$  dielectric phase is due to the  $\text{Bi}^{3+}$  ions from superfluous  $\text{Bi}_2\text{O}_3$  aids combining  $\text{Fe}^{3+}$  and  $\text{O}^{2-}$  ions [28,29]. With more  $\text{Sr}^{2+}$  ion substitutions, the

peak phase of the  $\text{Co}_{(2)}\text{Z}$  ferrites shifts towards a higher angle direction, indicating that the lattice constant decreases with the increase in  $\text{Sr}^{2+}$  ion content, according to the relationship between the phase and lattice constant [30,31].

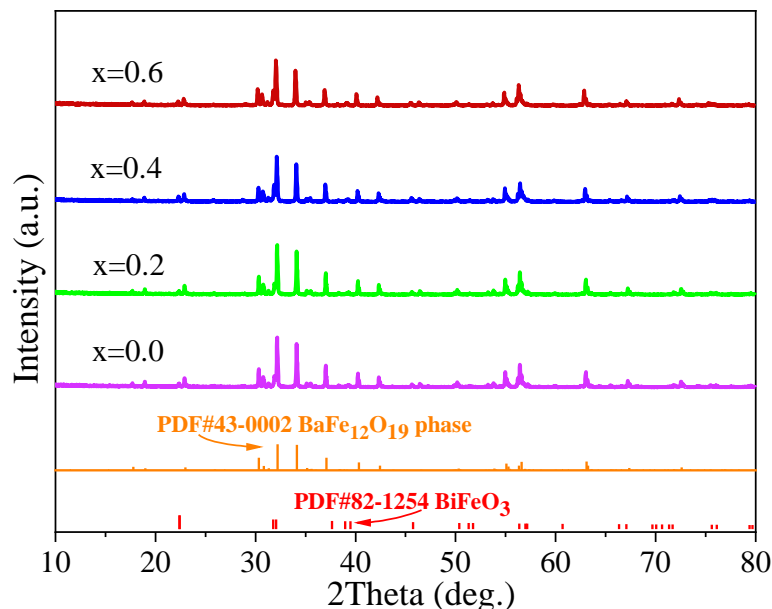


**Figure 2.** XRD patterns of ferrites with different  $\text{Sr}^{2+}$  ion substitution  $x$  values.

### 3.3. Magnetic and Dielectric Properties

Figure 3 shows the magnetic hysteresis loops and magnetic properties of samples sintered at five different temperature points ( $x = 0.0, 0.2, 0.4$  and  $0.6$ ). The magnetic hysteresis loops in Figure 3a indicate that the  $\text{Sr}^{2+}$  ion-substituted barium ferrites have excellent soft magnetic properties at low temperature. The loops also indicate that the magnetisation slightly weakened as  $x$  increased from  $0.0$  to  $0.6$ . The coercivity and saturation magnetisation value can be induced based on the loops. As shown in Figure 3b, the saturation magnetisation ( $M_s$ ) decreased from  $39.99$  to  $38.11$  emu/g when  $x$  increased from  $0.0$  to  $0.6$ . Meanwhile, coercivity ( $H_c$ ) increased from  $59.05$  to  $65.21$  Oe when  $x$  increased from  $0.0$  to  $0.6$ . The decrease in saturation magnetisation could be attributed to the decrease in grain size, according to the Neel theory of two sublattices [32], whereas the coercivity changes with inverse proportion to the saturation magnetisation. Their relationship is indicated by the following equation [33,34]:

$$M_s = \frac{0.96K}{H_c} \quad (3)$$

where  $M_s$  is saturation magnetisation,  $K$  is a dependence constant, and  $H_c$  is coercivity. Frequently, larger grain size conducts lower coercivity due to domain wall pinning that requires high energy for switching [35].

Figure 4 shows the complex magnetic permeability and complex dielectric permittivity of the  $\text{Co}_{(2)}\text{Z}$  ferrites substituted by  $\text{Sr}^{2+}$  ions. As  $\text{Sr}^{2+}$  ions increased, the real part of the magnetic permeability ( $\mu'$ ) hardly changed, whereas the imaginary part of the magnetic permeability ( $\mu''$ ) remained at a low value ( $\sim 0.2$  for all samples). According to the magnetic tangent  $\tan\delta_\mu$  equation definition [23], as follows:

$$\tan\delta_\mu = \mu''/\mu', \quad (4)$$

an ultra-low order of magnitude of  $\tan\delta_\mu$  (approximately  $8 \times 10^{-2}$ ) can be obtained over a long frequency band from  $1$  MHz to  $1$  GHz.  $\tan\delta_\mu$  is a valuable factor for the antenna substrate materials. Herein,  $\tan\delta_\mu$  is derived from three factors, namely the eddy current

loss tangent  $\tan\delta_e$ , the hysteresis loss tangent  $\tan\delta_a$  and the remaining loss tangent  $\tan\delta_c$ ; their relationship is as follows [8]:

$$\tan\delta_\mu = \tan\delta_e + \tan\delta_a + \tan\delta_c \quad (5)$$

where  $\tan\delta_e$  generated from the electro-magnetic induction, causing cover fever and generating power dissipation, is closely correlated with the coercivity ( $H_c$ ), and the  $\text{Fe}_3\text{O}_4$  particles are scattered between the crystals. In addition,  $\tan\delta_e$  can be affected by existing pores and changing grain size.  $\tan\delta_a$  can be tailored by changing the hysteresis constant, which reduces the hysteresis loop and  $H_c$ . The remaining loss tangent  $\tan\delta_c$  mainly relies on the ideal microstructure of the materials with dense arrangement, uniform thickness, border crystal boundary and pores. In this research, the low magnetic loss is attributed to the low-temperature sintered technology, and the appropriate sintering aids  $\text{Bi}_2\text{O}_3$ . However, for complex dielectric permittivity, the actual part ( $\epsilon'$ ) increased from approximately 8 to 12 when the  $x$  value increased from 0.0 to 0.6. The dielectric constant increases with increased  $\text{Sr}^{2+}$  ions based on Koop's phenomenological theory, in which the microstructure is regarded as a non-uniform intermediary of two layers, based on the Maxwell–Wagner type [36]. According to the theory, the dielectric construction of ferrites is composed of high- and low-conductivity grain grain boundaries. The high-conductivity grains are separated by grain boundaries, resulting in the localised build-up of charge carriers that increase interfacial polarisation. As a result,  $\epsilon'$  increases. As  $\text{Sr}^{3+}$  substitution content increases, the ability of the separation between the two layers is enhanced, and interfacial polarisation is further excited, resulting in an increase in  $\epsilon'$  [37]. In addition, reports showed a strong correlation between the conduction mechanism and the dielectric behaviour of the ferrites, starting with the supposition that the mechanism of the polarisation process in ferrites is similar to that of the conduction process. The electronic exchange in  $\text{Fe}^{2+} \Leftrightarrow \text{Fe}^{3+}$  results in local displacement that determines the polarisation of the ferrites. More electronic exchange occurs in  $\text{Fe}^{2+} \Leftrightarrow \text{Fe}^{3+}$  with the increase in  $\text{Sr}^{2+}$  ion content, resulting in higher local displacement that enhances dielectric properties [38]. Meanwhile, the imaginary part of the dielectric permittivity ( $\epsilon''$ ) was approximately 0.5 to 0.1 over the frequency of 1 MHz to 1 GHz. As a consequence, the dielectric loss  $\tan\delta_\epsilon$  was calculated (similar to that of  $\tan\delta_\mu$ ) to be approximately 0.007 in all samples. This value is also fairly low amongst ferrite ceramic materials. In general,  $\tan\delta_\epsilon$  is closely related to two factors: (i) the crystal grain boundaries and ferrite polycrystallinity and (ii) the microstructure including porosity and grain size. Their relationship can be expressed by the following equation [39]:

$$\tan\delta_\epsilon = (1 - P)\tan\delta_0 + CP^n \quad (6)$$

where  $\tan\delta_0$  is the dielectric loss of materials with completely dense microstructure,  $P$  is the porosity, and  $C$  is a dependent constant. In Equation (4),  $\tan\delta_\epsilon$  is mainly determined by  $P$ , which depends on relatively low porosity. In this work, high temperature enabled  $\text{Bi}_2\text{O}_3$  to form molten  $\text{BiFeO}_3$  dielectric crystals that could fill the void between grains. Thus, the structures became denser, mainly causing low dielectric loss. In general, when  $\tan\delta_\mu$  and  $\tan\delta_\epsilon$  are remarkably reduced, the proposed ferrite materials still exhibit excellent application prospects as antenna substrates.

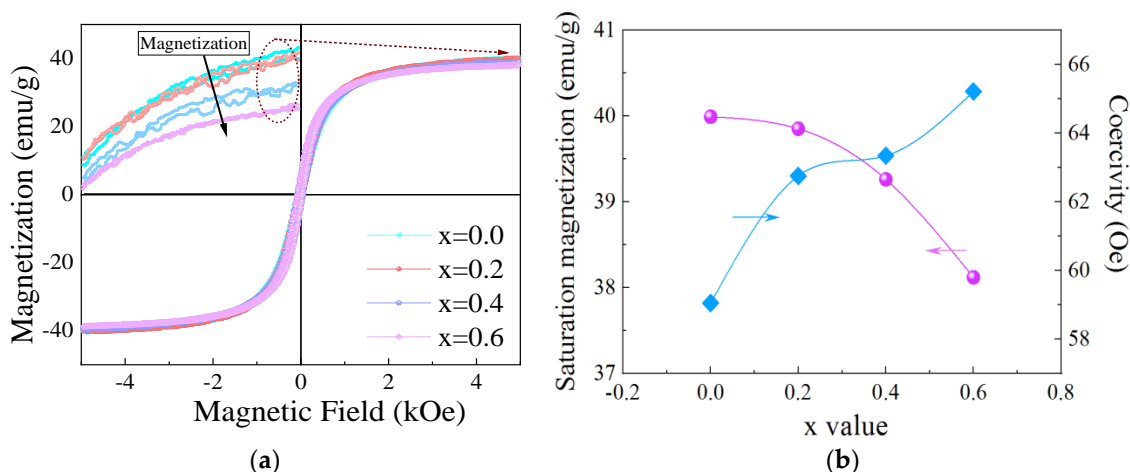


Figure 3. Magnetic hysteresis loops. (a) Magnetic properties and (b) samples sintered with various Sr<sup>2+</sup> ion substitution.

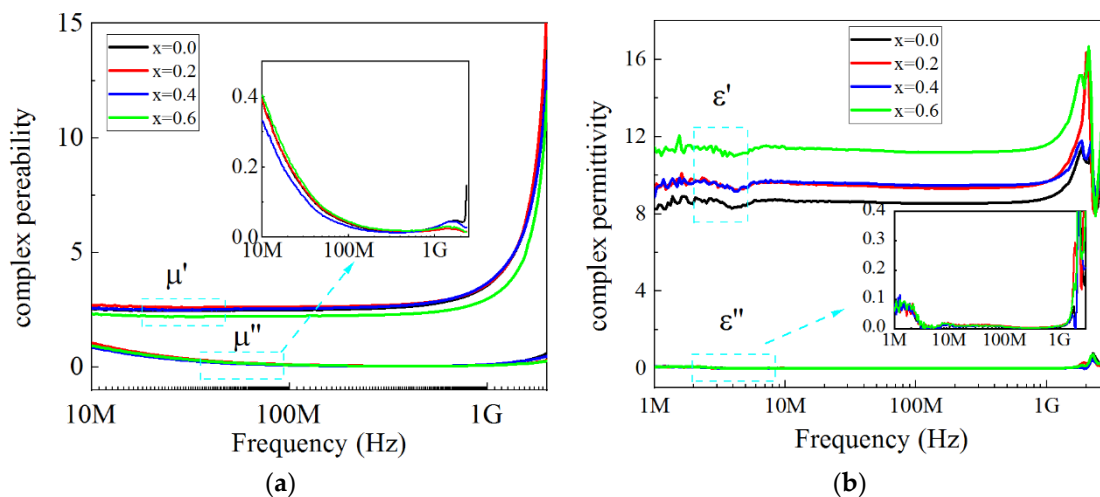
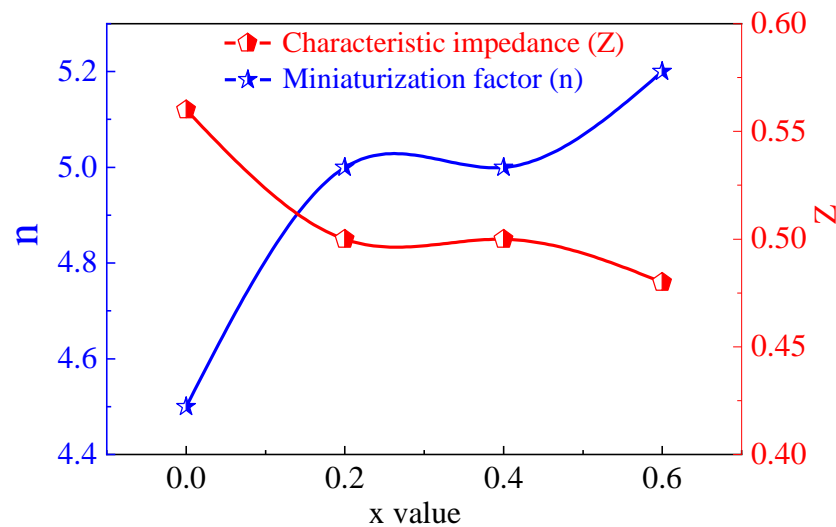


Figure 4. Complex magnetic permeability. (a) Complex dielectric permittivity (b) and samples with various x values.

The permeability and permittivity of all the samples in Figure 4 show that the actual parts of permeability and permittivity had similar values in the experimental scope. The miniaturisation factor ( $n$ , refractive index) and relative impedance ( $Z$ ) of CO<sub>2</sub>Z ferrites with various Sr<sup>3+</sup> ions substituted were calculated and are shown in Figure 5 and Table 1. The results show that  $n$  increases monotonically, and  $Z$  decreases with the increase in  $x$  value. However,  $Z$  decreases by much less than  $n$  increases. Finally, the sample substituted by Sr<sup>3+</sup> ions with an  $x$  value of 0.6 exhibited the most ideal properties through comparison and consideration of various trade-offs.

Table 1. Miniaturisation factor ( $n$ , refractive index) and relative impedance ( $Z$ ) of CO<sub>2</sub>Z ferrites corresponding to various  $x$  values.

$x$ Value	0.00	0.20	0.40	0.60
$n$ value	4.5	5	5	5.2
$Z$ value	0.56	0.50	0.50	0.48



**Figure 5.** Miniaturisation factor ( $n$ ) and relative impedance ( $Z$ ) of  $\text{CO}_{(2)}\text{Z}$  ferrites with various  $x$  values.

#### 4. Conclusions

In this study, superfluous  $\text{Bi}_2\text{O}_3$  sintering aids were added to various  $\text{Sr}^{3+}$  ion-substituted  $\text{CO}_{(2)}\text{Z}$  ferrites to achieve low-temperature sintering. The ferrites were made up of two phases and showed changing magnetic and dielectric properties, thereby approaching equal permeability and permittivity values. When the  $x$  value was 0.6, the materials had the topmost permittivity values ( $\epsilon' \approx 12$ ), whereas  $\mu'$  was barely changed. As a result, larger  $n$  and appropriate  $Z$  could be obtained. Meanwhile, low magnetic loss ( $\tan\delta_\mu \approx 0.08$ ) and low dielectric loss ( $\tan\delta_\epsilon \approx 0.007$ ) indicate low power loss during operation. The results showed that the  $\text{Sr}^{3+}$  ions enhanced dielectric properties, indicating that  $\text{CO}_{(2)}\text{Z}$  ferrite can be an excellent candidate for high-frequency antenna substrates.

**Author Contributions:** Conceptualization, J.W. and G.G.; methodology, K.L.; software, J.W.; validation, K.L. and G.G.; formal analysis, J.W.; investigation, J.W.; resources, K.L.; data curation, J.W.; writing—original draft preparation, J.W.; writing—review and editing, G.G.; visualization, K.L.; supervision, G.G.; project administration, K.L.; funding acquisition, G.G. All authors have read and agreed to the published version of the manuscript.

**Funding:** This research received no external funding.

**Institutional Review Board Statement:** Not applicable.

**Informed Consent Statement:** Not applicable.

**Data Availability Statement:** The raw/processed data required to reproduce these findings cannot be shared at this time as the data also form part of an ongoing study.

**Conflicts of Interest:** The authors declare no conflict of interest. We declare that we do not have any commercial or associative interest that represents a conflict of interest in connection with the work submitted.

#### References

- Saini, A.; Rana, K.; Thakur, A.; Thakur, P.; Mattei, J.L.; Queffelec, P. Low loss composite nano ferrite with matching permittivity and permeability in UHF band. *Mater. Res. Bull.* **2016**, *76*, 94–99. [[CrossRef](#)]
- Mattei, J.L.; Souriou, D.; Chevalier, A. Magnetic and dielectric properties in the UHF frequency band of half-dense Ni-Zn-Co ferrites ceramics with Fe-excess and Fe-deficiency. *J. Magn. Magn. Mater.* **2018**, *447*, 9–14. [[CrossRef](#)]
- Dar, M.A.; Varshney, D. Effect of d-block element  $\text{Co}^{2+}$  substitution on structural, Mössbauer and dielectric properties of spinel copper ferrites. *J. Magn. Magn. Mater.* **2017**, *436*, 101–112. [[CrossRef](#)]
- Peng, Y.; Wu, X.; Chen, Z.; Liu, W.; Wang, F.; Wang, X.; Feng, Z.; Chen, Y.; Harris, V.G.  $\text{BiFeO}_3$  tailored low loss M-type hexaferrite composites having equivalent permeability and permittivity for very high frequency applications. *J. Alloys Compd.* **2015**, *630*, 48–53. [[CrossRef](#)]

5. Joulaei, M.; Hedayati, K.; Ghanbari, D. Investigation of magnetic, mechanical and flame retardant properties of polymeric nanocomposites: Green synthesis of  $\text{MgFe}_2\text{O}_4$  by lime and orange extracts. *Compos. Part B Eng.* **2019**, *176*, 107345. [[CrossRef](#)]
6. Reddy, M.P.; Shakoor, R.A.; Mohamed, A.M.A.; Gupta, M.; Huang, Q. Effect of sintering temperature on the structural and magnetic properties of  $\text{MgFe}_2\text{O}_4$  ceramics prepared by spark plasma sintering. *Ceram. Int.* **2016**, *42*, 4221–4227. [[CrossRef](#)]
7. Zu, Y.; Zhao, Y.; Xu, K.; Tong, Y.; Zhao, F. Preparation and comparison of catalytic performance for nano  $\text{MgFe}_2\text{O}_4$ , GO-loaded  $\text{MgFe}_2\text{O}_4$  and GO-coated  $\text{MgFe}_2\text{O}_4$  nanocomposites. *Ceram. Int.* **2016**, *42*, 18844–18850. [[CrossRef](#)]
8. Peng, Y.; Wu, X.; Chen, Z.; Li, Q.; Yu, T.; Feng, Z.; Su, Z.; Chen, Y.; Harris, V.G. High frequency permeability and permittivity spectra of  $\text{BiFeO}_3/(\text{CoTi})\text{-BaM}$  ferrite composites. *J. Appl. Phys.* **2015**, *117*, 17A306. [[CrossRef](#)]
9. Thakur, A.; Thakur, P.; Hsu, J.H. Novel magnetodielectric nanomaterials with matching permeability and permittivity for the very-high-frequency applications. *Scr. Mater.* **2011**, *64*, 205–208. [[CrossRef](#)]
10. Yu, S.H.; Yoshimura, M. Ferrite/metal composites fabricated by soft solution processing. *Adv. Funct. Mater.* **2002**, *12*, 9–15. [[CrossRef](#)]
11. Nasrin, S.; Khan, S.M.; Matin, M.A.; Khan, M.N.I.; Hossain, A.K.M.A.; Rahaman, M.D. Synthesis and deciphering the effects of sintering temperature on structural, elastic, dielectric, electric and magnetic properties of magnetic  $\text{Ni}_{0.25}\text{Cu}_{0.13}\text{Zn}_{0.62}\text{Fe}_2\text{O}_4$  ceramics. *J. Mater. Sci. Mater. Electron.* **2019**, *30*, 10722–10741. [[CrossRef](#)]
12. Manhas, A.; Batoo, K.M.; Singh, M. Magnetic and Mössbauer investigations of soft Co2Z-type hexa nanoferrites. *J. Alloys Compd.* **2018**, *767*, 188–194. [[CrossRef](#)]
13. Lee, W.; Hong, Y.K.; Park, J.; Larochele, G.; Lee, J. Low-loss Z-type hexaferrite ( $\text{Ba}_3\text{Co}_2\text{Fe}_{24}\text{O}_{41}$ ) for GHz antenna applications. *J. Magn. Magn. Mater.* **2016**, *414*, 194–197. [[CrossRef](#)]
14. Xu, F.; Bai, Y.; Qiao, L.; Zhao, H.; Zhou, J. Realization of negative permittivity of Co2Z hexagonal ferrite and left-handed property of ferrite composite material. *J. Phys. D Appl. Phys.* **2009**, *42*, 025403. [[CrossRef](#)]
15. Bae, S.; Hong, Y.K.; Lee, J.J.; Jalli, J.; Abo, G.S.; Lyle, A.; Seong, W.M.; Kum, J.S. Low loss Z-type barium ferrite (Co2 Z) for terrestrial digital multimedia broadcasting antenna application. *J. Appl. Phys.* **2009**, *105*, 07A515. [[CrossRef](#)]
16. Chang, H.; Lee, H.B.; Chung, J.H.; Chun, S.H.; Shin, K.W.; Jeon, B.G.; Kim, K.H.; Prokeš, K.; Mat'aš, S. Commensurate transverse helical ordering in the room-temperature magnetoelectric Co2Z hexaferrite. *Phys. B Condens. Matter.* **2018**, *551*, 122–126. [[CrossRef](#)]
17. Karimi-Maleh, H.; Karaman, C.; Karaman, O.; Karimi, F.; Vasseghian, Y.; Fu, L.; Baghayeri, M.; Rouhi, J.; Kumar, P.S.; Show, P.-L.; et al. Nanochemistry approach for the fabrication of Fe and N co-decorated biomass-derived activated carbon frameworks: A promising oxygen reduction reaction electrocatalyst in neutral media. *J. Nanostruct. Chem.* **2022**, *12*, 429–439. [[CrossRef](#)]
18. Al Sharabati, M.; Abokwiek, R.; Al-Othman, A.; Tawalbeh, M.; Karaman, C.; Orooji, Y.; Karimi, F. Biodegradable polymers and their nano-composites for the removal of endocrine-disrupting chemicals (EDCs) from wastewater: A review. *Environ. Res.* **2021**, *202*, 111694. [[CrossRef](#)]
19. Karimi-Maleh, H.; Khataee, A.; Karimi, F.; Baghayeri, M.; Fu, L.; Rouhi, J.; Karaman, C.; Karaman, O.; Boukherroub, R. A green and sensitive guanine-based DNA biosensor for idarubicin anticancer monitoring in biological samples: A simple and fast strategy for control of health quality in chemotherapy procedure confirmed by docking investigation. *Chemosphere* **2022**, *291*, 132928. [[CrossRef](#)]
20. Yarhmadi, M.; Maleki-Ghaleh, H.; Mehr, M.E.; Dargahi, Z.; Rasouli, F.; Siadati, M.H. Synthesis and characterization of Sr-doped ZnO nanoparticles for photocatalytic applications. *J. Alloys Compd.* **2021**, *853*, 157000. [[CrossRef](#)]
21. Hu, Z.Z.; Lu, J.J.; Chen, B.H.; Liu, X.Q.; Chen, X.M. Improved ferroelectric properties in hybrid improper ferroelectric  $\text{Sr}_{3-x}\text{Ba}_x\text{Zr}_2\text{O}_7$ . *J. Alloys Compd.* **2021**, *866*, 158705. [[CrossRef](#)]
22. Gan, G.; Zhang, H.; Li, Q.; Li, J.; Li, M.; Xu, F.; Jing, Y.  $\text{Bi}_2\text{O}_3$  enhances magnetic and dielectric properties of low temperature co-fired  $\text{Ba}(\text{CoTi})_{1.20}\text{Fe}_{9.6}\text{O}_{19}$  ferrite composites in an oxygen atmosphere for applications in high frequency antennas. *Mater. Res. Bull.* **2018**, *97*, 37–41. [[CrossRef](#)]
23. Gan, G.; Zhang, H.; Li, Q.; Li, J.; Huang, X.; Xie, F.; Xu, F.; Zhang, Q.; Li, M.; Liang, T.; et al. Low loss, enhanced magneto-dielectric properties of  $\text{Bi}_2\text{O}_3$  doped Mg-Cd ferrites for high frequency antennas. *J. Alloys Compd.* **2018**, *735*, 2634–2639. [[CrossRef](#)]
24. Gan, G.; Zhang, D.; Li, J.; Wang, G.; Huang, X.; Rao, Y.; Yang, Y.; Wang, X.; Zhang, H.; Chen, R.T. Ga ions-tailored magnetic-dielectric properties of Mg-Cd composites for high-frequency, miniature and wideband antennas. *Ceram. Int.* **2020**, *46*, 8398–8404. [[CrossRef](#)]
25. Gan, G.; Zhang, D.; Li, J.; Wang, G.; Huang, X.; Yang, Y.; Rao, Y.; Wang, X.; Zhang, H.; Chen, R.T. Low-loss Cd-substituted Mg ferrites with matching impedance for high-frequency-range antennas. *J. Magnes. Alloy.* **2021**, *9*, 1396–1405. [[CrossRef](#)]
26. Li, Q.; Yan, S.; Wang, X.; Nie, Y.; Feng, Z.; Su, Z.; Chen, Y.; Harris, V.G. Dual-ion substitution induced high impedance of Co2Z hexaferrites for ultra-high frequency applications. *Acta Mater.* **2015**, *98*, 190–196. [[CrossRef](#)]
27. Yang, P.; Qi, H.; Liu, Z.; Fu, X.; Peng, Z. Microstructure, magnetism, and high-frequency performance of polycrystalline  $\text{Ni}_{0.5}\text{Zn}_{0.5}\text{Sm}_{0.025}\text{HoxFe}_{1.975-x}\text{O}_4$  ferrites. *J. Am. Ceram. Soc.* **2019**, *102*, 7469–7479. [[CrossRef](#)]
28. Li, Q.; Bao, S.; Liu, Y.; Li, Y.; Jing, Y.; Li, J. Influence of lightly Sm-substitution on crystal structure, magnetic and dielectric properties of  $\text{BiFeO}_3$  ceramics. *J. Alloys Compd.* **2016**, *682*, 672–678. [[CrossRef](#)]
29. Hao, P.; Zhao, Z.; Tian, J.; Sang, Y.; Yu, G.; Liu, H.; Chen, S.; Zhou, W. Bismuth titanate nanobelts through a low-temperature nanoscale solid-state reaction. *Acta Mater.* **2014**, *62*, 258–266. [[CrossRef](#)]

30. Ghosh, M.P.; Mukherjee, S. Microstructural, magnetic, and hyperfine characterizations of Cu-doped cobalt ferrite nanoparticles. *J. Am. Ceram. Soc.* **2019**, *102*, 7509–7520. [[CrossRef](#)]
31. Xu, F.; Liao, Y.; Zhang, D.; Zhou, T.; Li, J.; Gan, G.; Zhang, H. Synthesis of Highly Uniform and Compact Lithium Zinc Ferrite Ceramics via an Efficient Low Temperature Approach. *Inorg. Chem.* **2017**, *56*, 4512–4520. [[CrossRef](#)] [[PubMed](#)]
32. Samajdar, R.; Scheurer, M.S.; Chatterjee, S.; Guo, H.; Xu, C.; Sachdev, S. Enhanced thermal Hall effect in the square-lattice Néel state. *Nat. Phys.* **2019**, *15*, 1290–1294. [[CrossRef](#)]
33. Qiu, C.; Lu, T.; He, F.; Feng, S.; Fang, X.; Zuo, F.; Jiang, Q.; Deng, X.; Ye, J. Influences of gallium substitution on the phase stability, mechanical strength and cellular response of  $\beta$ -tricalcium phosphate bioceramics. *Ceram. Int.* **2020**, *46*, 16364–16371. [[CrossRef](#)]
34. Trukhanov, A.V.; Trukhanov, S.V.; Kostishyn, V.G.; Panina, L.V.; Kazakevich, I.S.; Trukhanov, A.V.; Natarov, V.O.; Chitanov, D.N.; Turchenko, V.A.; Oliynyk, V.; et al. Microwave properties of the Ga-substituted BaFe<sub>12</sub>O<sub>19</sub> hexaferrites. *Mater. Res. Express* **2017**, *4*, 076106. [[CrossRef](#)]
35. Shinde, V.S.; Dahotre, S.G.; Singh, L.N. Synthesis and characterization of aluminium substituted calcium hexaferrite. *Heliyon* **2020**, *6*, e03186. [[CrossRef](#)]
36. Naik, C.C.; Salker, A.V. Effect Cr<sup>3+</sup> Ion Substitution on the Structural, Magnetic, and Dielectric Behavior of Co–Cu Ferrite. *J. Supercond. Nov. Magn.* **2019**, *32*, 3655–3669. [[CrossRef](#)]
37. Sathishkumar, G.; Venkataraju, C.; Sivakumar, K. Magnetic and dielectric properties of cadmium substituted nickel cobalt nanoferrites. *J. Mater. Sci. Mater. Electron.* **2013**, *24*, 1057–1062. [[CrossRef](#)]
38. Kumar, B.R.; Ravinder, D. Dielectric properties of Mn-Zn-Gd ferrites. *Mater. Lett.* **2002**, *53*, 437–440. [[CrossRef](#)]
39. Krishnaveni, T.; Murthy, S.R.; Gao, F.; Lu, Q.; Komarneni, S. Microwave hydrothermal synthesis of nanosize Ta<sub>2</sub>O<sub>5</sub> added Mg-Cu-Zn ferrites. *J. Mater. Sci.* **2006**, *41*, 1471–1474. [[CrossRef](#)]